Journal of Heat and Mass Transfer Research

Journal homepage: http://jhmtr.semnan.ac.ir

Semnan University

Analytical Solution of Non-ideal Gaseous Slip Flow in Circular Sector Micro-channel

Mahdi Motamedian, Ahmad Reza Rahmati *

Department of Mechanical Engineering, University of Kashan, Iran.

PAPER INFO

Paper history:
Received: 2019-11-15
Revised: 2020-06-05
Accepted: 2020-06-16

Keywords:
Slip flow;
Microchannel;
Circular sector;
Integral transform;
Conformal mapping.

ABSTRACT

Analytical solutions of gaseous slip flow in a microchannel with different cross-sections play an important role in the understanding of the physical behavior of gases and other phenomena related to it. In this paper, the fully developed non-ideal gaseous slip flow in circular sector microchannel is investigated using the conformal mapping and the integral transform technique to obtain the analytical exact solution. Van der Waals equation is used as the equation of state for a non-ideal gas.It is developed the models for predicting the local and mean velocity, normalized Poiseuille number,and the ratio of density for conditions where the small radius of the circular sector cross-section is zero ($r_1^*\to 0$) and is the opposite of zero ($r_1^*\neq 0$, $r_1^*=10\mu m$).Rarefication process and effects of wall slippage are important physical phenomena that are studied. The results show that the rarefication process depends on Knudsen number, and cross-section geometry. In order to validate the analytical solution, the results of the problem are compared to the analytical and numerical solutions. Good agreement between the present study and other solutions has confirmed.

DOI: 10.22075/jhmtr.2020.19129.1259

1. Introduction

In the past years, extensive studies have been conducted on fluid flow in microfluidic devices. The engineering applications of microfluidic devices include micro power plant, micro engines, cooling of a microelectronic circuit, digital micro-compressors, high-frequency fluidic control systems, fuel cell technology, high heat-flux compact heat exchanger and so on.

Important applications of the gas flow in a microchannel are known as gas chromatography, micro chemical gas reactor, microscale heat exchanger and micro gas regulators, ultrasensitive gas flow sensors. Few studies have been carried out in the analytical solution of gaseous slip flow in micro-channel and are mainly limited to ideal gas flow and micro-channel with simple cross-section such as rectangular, squares and circular. Todays, microchannels are fabricated with various cross-sectional geometry. Therefore, it is important to represent an analytical solution of non-ideal gaseous slip flow for microchannels with complex cross-sections to investigate the physical behavior of gases. For the specific problem presented in this paper, there has been no analytical solution based on differential formulation so far. Arkilic et al.[1] analytically and experimentally analyzed gaseous flow in a two-dimensional long microchannel by using Navier-Stokes equations. They demonstrated the effects of compressibility and rarefication.An analysis of rarefied gas flows in rectangular and annular ducts has been performed using an analytical method by Ebert and Sparrow [2]. The results show that the effects of slip decrease velocity distribution and pressure drop are increased by the effect of compressibility. Zohar et al.[3] studied compressible subsonic ideal gas flow in a two-dimensional microchannel using the Navier- Stokes equations, analytically and experimentally. Their results were excellent agreements with the results of Arklik et al.[1].

Ideal gas flow was analyzed in a two-dimensional rectangular microchannel by Shen et al.[4].

They used degenerated Reynolds equation. The results were a good agreement with the DSMC numerical method.

*Corresponding Author: Ahmad Reza Rahmati, Department of Mechanical Engineering, University of Kashan, Iran.
Email: ar_rahmati@kashanu.ac.ir

The rarefaction effects on the pressure drop for incompressible flow in a silicon rectangular, trapezoidal or double-trapezoidal cross-section are evaluated by Morini et al.[5].The effects of the Knudsen number and the cross-section aspect ratio in the friction factor reduction is discussed. Dongari et al.[6] studied analytically ideal gas flow in a two-dimensional rectangular microchannel with the integral form of the Navier-Stokes equations. Their results are compared with the first-order boundary conditions and also less dependent on the Reynolds number. Also, their solution was considered as the most general solution for gas flow in long microchannel[7]. They analyzed analytically a gas flow in a two-dimensional microchannel which included the mass flux term with non-slip boundary conditions and compared with the experimental results [8, 9]. Also, the isothermal gas flow was investigated in a two-dimensional microchannel in the continuous flow up to the transitional regime by Navier Stokes equations with the first-order Maxwell slip boundary conditions [10].

Wimmer et al.[11] used Laplace transform method to examine gas flow in two parallel plates. They used the Oseen equation to investigate the flow and compared the results with the numerical method. Duan et al.[12, 13] investigated a slip-flow through the non-circular and elliptic microchannels. The results show that the accuracy of the developed model is 10% and 3% for elliptic and non-circular microchannels respectively. Rashidi et al.[14] analyzed an ideal gas flow in a two-dimensional rectangular microchannel by the VIM method and compared the accuracy and convergence of the VIM method with the numerical solution. Das and Tahmouresi[15] studied an ideal fully developed gaseous flow in an elliptic microchannel by using the integral transform technique. They investigated the effect of duct shape. The results show that normalized Poiseuille, friction factor and Reynolds number are good improvement with the previous results of rectangular and elliptic microchannels.

kurkin et al.[16] simulated an ideal gas flow in a uniform two-dimensional microchannel, Their results indicate that there is a good agreement between analytical and numerical solution in velocity and pressure profiles. Duan and Yovanovich[17] represented a simple model to predict the friction factor and Reynolds number product in different cross-section microchannels for slip flow. The results show that the accuracy of Poiseuille number is 4.2% for all common duct shapes. Ihle and Kroll[18] analyzed a non-ideal gas flow in a microchannel. They proposed several distribution functions to show the non-ideal gas and potential energy effects in the thermal lattice Boltzmann method with potential energy. Reddy and Reddy[19] drove an analytical solution to investigate the effect of velocity slip and Joule heating on peristaltic flow of MHD Newtonian fluid in a porous channel with elastic wall properties. They discussed the emerging flow parameters on the velocity, temperature and heat transfer coefficient. Gas flow in a circular microchannel with a sudden expansion was analyzed by Huang and Lu[20]. They used the lattice Boltzmann method. The results show good agreement with an analytical solution for smooth and straight circular microchannel. Tahmouresi and Das[21] presented the fully developed gaseous slip-flow in symmetric and non-symmetric parabolic micro-channels by applying the method of separation of variables. Normalized Poiseuille number, mass flow rate, and pressure distribution are compared with previous results. For a small aspect ratio, it is found that results are a good agreement with rectangular micro-channels. Huang et al.[22] examined a gas flow in a long circular microchannel using the lattice Boltzmann method. The results show that with the increase of Pr, the compressibility effects increase. A rarefied gas flow model in a long circular microchannel with different input and output pressure ratios at low Mach numbers was carried out Yang and Garimella[23].The model shows that there is a good agreement between these two methods in the mass flow rate and pressure drop.

Hong et al.[24] experimentally evaluated nitrogen flow through a rectangular microchannel with silicon wafers and capped with glass surface properties. It was performed to achieve the local values of Mach number, temperature and friction factor. When stagnation pressure due to flow acceleration increases, the pressure and temperature decrease and the Mach number improves. In through the microchannel, with increasing the Reynolds number, the value of sudden rises. Li and Hrnjak[25] investigated the effect of the channel's diameter and length of the flow through microchannel evaporators, experimentally and numerically. It was found that the larger channel diameter and longer channel reveal less flow reversal with a lower frequency. In another study, they analyzed the effect of refrigerant specific volume differences and heat of vaporization on flow in microchannel evaporators. Their results show that fluids with lower heat of vaporization and higher specific volume difference between vapor and liquid phase produce more reversed vapor flow[26]. Monsivais et al.[27] presented asymptotically and numerically the conjugate heat transfer creep between a rarified gas flow and the lower wall of a thin horizontal microchannel. The results show that the velocity and temperature profiles for the gas phase and the temperature profiles for the solid wall are predicted as functions of the involved dimensionless parameters and the main results confirm that the phenomenon of conjugate thermal creep exists whenever the temperature of the lower wall varies linearly or nonlinearly. Das et al.[28] numerically investigated the free convective slip flow of a viscous incompressible couple–stress fluid in a vertical stretching sheet with thermal radiation. The results show that fluid velocity improves due to the buoyancy force and reduces due to thermal radiation. Thermal boundary layer thickness is the function of the thermal radiation and the Prandtl number. When the values of Grashof number increases, the momentum boundary layer thickness reduces. Sarojamma et al.[29] analyzed the effects of non-

Newtonian rheology, slip velocity, thermal radiation, heat generation/absorption, and first-order chemical reactions on the unsteady MHD mixed convective heat and mass transfer of an incompressible Casson fluid over a wedge under the influence of a magnetic field. The results show that increasing the values of the Casson Parameter leads to improve the values of velocity, temperature, and reduce the concentration. Also, the slip parameters increase the velocity and decrease the temperature and species concentration. Rahmati and Nejati[30] presented the analytical solution for incompressible thermal flow in a micro-Couette under the transition regime. They used the Burnett equations with first-and second-order slip boundary conditions. The results show that an increasing Knudsen number increases the slip on the wall, Poiseuille, and Nusselt numbers and decreases the curvature of the profile.

In this paper, a fully developed non-ideal gas flow through a circular sector microchannel is analytically analyzed. This study takes on the application of conformal mapping to solve the momentum equation(namely Laplace and Poisson) using integral transform technique. The effects of wall slippage in the range of slip flow regime have been investigated. Firstly, the general problem will be introduced to demonstrate the governing equations, the geometry of fluid flow and boundary condition equations. Secondly, the method will be applied in the circular sector microchannel with Robin boundary condition and the results will be validated by the exact solution and numerical solution. Finally, the results will be discussed.

2. Analytical solution

A fully developed gaseous slip flow is considered in a straight circular sector microchannel with a uniform cross-section(Fig.1a). In this study, the assumptions of the gaseous slip flow include the fully developed, steady-state, laminar, compressible and constant fluid physical properties. Body force is neglected and the momentum equation in z-axis(coincides with the main flow direction) is:

$$\frac{\partial^2 u}{\partial x^{*2}} + \frac{\partial^2 u}{\partial y^{*2}} = \frac{1}{\mu}\frac{dp}{dz} \tag{1}$$

Barron *et al.*[31] and Maxwell[32] have been represented the slip velocity for gas flow in the directions parallel to the wall:

$$u = u_s = -\beta_v \lambda \frac{\partial u}{\partial n^*} \tag{2}$$

β_v is defined:

$$\beta_v = \frac{2-\sigma_v}{\sigma_v} \tag{3}$$

In Eqs(2), u_s, β_v, σ_v, λ and n^* are defined as the slip velocity, the general slip parameter, the tangential momentum accommodation coefficient ($\sigma_v = (0.87 - 1)$ [33]), the molecular mean free path and normal direction to the wall of dimensional circular sector microchannels.

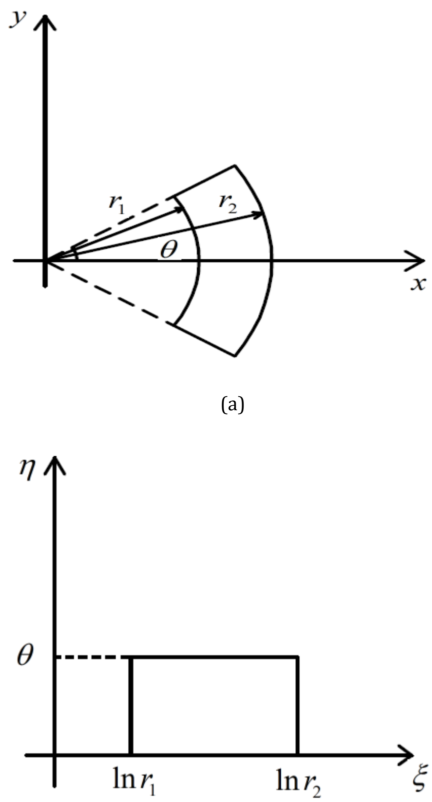

(a)

(b)

Figure 1. (a) Gas flow in circular sector microchannel, (b) Dimentionless transferred microchannel

2.1. Non-dimensional parameters

Considering non-dimensionless the following parameters:

$$x = \frac{x^*}{\sqrt{A_c}} \tag{4}$$

$$y = \frac{y^*}{\sqrt{A_c}} \tag{5}$$

$$r = \frac{r^*}{\sqrt{A_c}} \tag{6}$$

$$n = \frac{n^*}{\sqrt{A_c}} \tag{7}$$

$$\theta = \theta^* \tag{8}$$

In above equation(Eqs.(4)-(8)), A_c is area of the cross-section of circular sector microchannels. Substituting Eqs.(4) and (5) into Eq.(1):

$$\frac{\partial^2 u}{\partial x^2} + \frac{\partial^2 u}{\partial y^2} = P \tag{9}$$

Where

$$P = \frac{(\sqrt{A_c})^2}{\mu}\frac{dp}{dz} \tag{10}$$

Also, Substituting Eq.(7) into Eq.(2):

$$u = u_s = -\beta_v Kn \frac{\partial u}{\partial n} \tag{11}$$

Knudsen number is defined as follows:

$$Kn = \frac{\lambda}{\sqrt{A_c}} \tag{12}$$

2.2. Mathematical Formulation

Arfken transform is considered to solve the momentum equation(Eq.(9)). Cylindrical coordinates (ξ,η, z) are defined in terms of Cartesian coordinates system (x,y,z) by:

$$\begin{cases} x = e^{\xi} cos\eta \\ y = e^{\xi} sin\eta \\ z = z \end{cases} \tag{13}$$

The coefficients h_ξ, h_η, h_z and Jacobian transform is defined as:

$$h_\xi = h_\eta = e^{\xi} \tag{14}$$

$$h_z = 1 \tag{15}$$

$$J = det \left| \frac{\partial(x,y)}{\partial(\xi,\eta)} \right| = e^{2\xi} \tag{16}$$

The infinitesimal element area is:

$$dA = e^{2\xi} d\xi d\eta \tag{17}$$

Substituting above equation in Eqs.(9) and applying boundary conditions for upper half cross- section microchannel, the momentum and boundary condition equations become:

$$\frac{\partial^2 u}{\partial \xi^2} + \frac{\partial^2 u}{\partial \eta^2} = e^{2\xi}.P \tag{18}$$

$$\frac{1}{h_\eta}\frac{\partial u}{\partial \eta} = 0 \qquad at\ \eta = 0 \tag{19}$$

$$u = \frac{-\beta_v Kn}{h_\eta}\frac{\partial u}{\partial \eta} \quad at\ \eta = \theta \tag{20}$$

$$u = \frac{-\beta_v Kn}{h_\xi}\frac{\partial u}{\partial \xi} \quad at\ \xi = lnr_1 \tag{21}$$

$$u = \frac{-\beta_v Kn}{h_\xi}\frac{\partial u}{\partial \xi} \quad at\ \xi = lnr_2 \tag{22}$$

Substituting Eq.(14) in to Eqs.(19)-(22):

$$\frac{\partial^2 u}{\partial \xi^2} + \frac{\partial^2 u}{\partial \eta^2} = e^{2\xi} P \tag{23}$$

$$\frac{\partial u}{\partial \eta} = 0 \qquad at\ \eta = 0 \tag{24}$$

$$u = -e^{-\xi}\beta_v Kn \frac{\partial u}{\partial \eta} \qquad at \eta = \theta \tag{25}$$

$$u = -e^{-\xi}\beta_v Kn \frac{\partial u}{\partial \xi} \qquad at\ \xi = lnr_1 \tag{26}$$

$$u = -e^{-\xi}\beta_v Kn \frac{\partial u}{\partial \xi} \qquad at\ \xi = lnr_2 \tag{27}$$

2.3. Method of Seperation of Variables

In this section, the homogeneous equation(Eq.(23)) is solved by applying the method of separation of variables and finally, a specific solution to the equation is obtained. Then,

$$\frac{\partial^2 u}{\partial \xi^2} + \frac{\partial^2 u}{\partial \eta^2} = 0 \tag{28}$$

To solve Eq.(28), it is assumed that velocity is a function of the product $X(\xi)$and $Y(\eta)$, then:

$$u(\xi,\eta) = X(\xi)Y(\eta) \tag{29}$$

Substituting Eq.(29) in to Eq.(28):

$$X''(\xi)Y(\eta) + X(\xi)Y''(\eta) = 0 \tag{30}$$

Defining :

$$\frac{X''(\xi)}{X(\xi)} = -\frac{Y''(\eta)}{Y(\eta)} = \delta^2 \tag{31}$$

From Eq.(31), the following equation is obtained:

$$Y''(\eta) + \delta^2 Y(\eta) = 0 \tag{32}$$

Solving Second-order homogeneous differential equation(Eq.(32)) is:

$$Y(\eta) = a_n cos(\delta_n \eta) + b_n sin(\delta_n \eta) \tag{33}$$

Applying the boundary condition Eqs.(24) and (25):

$$b_n = 0 \tag{34}$$

$$\delta_n tan(\delta_n \theta) = \frac{e^{\xi}}{\beta_v Kn} \tag{35}$$

From solving equation(Eq.(35)), The results show that the variations of the $\delta_n$are negligible with the variation of ζ and for different Knudsen number. then, $\delta_n$is independent of ζ and Knudsen number and its values are constant approximately (Table 1: δ_n=[-2.97,-2.99], δ_n=cte). If values of δ_n would be a function of ξ, η, the analytical solution would be difficult to solve.

Thus, Eq.(23) is converted to the following equation:

$$u(\xi,\eta) = \sum_{n=1}^{\infty} X_n(\xi) cos(\delta_n \eta) \tag{36}$$

Substituting Eq.(36) into Eq.(23), the following equation is obtained:

$$\sum_{n=1}^{\infty} (X''_n(\xi) - {\delta_n}^2 X_n(\xi)) \times cos(\delta_n \eta) = e^{2\xi} P \tag{37}$$

Using orthogonality principles [17], the following integral equation is represented:

$$\begin{aligned} (X''_n(\xi) - {\delta_n}^2 X_n(\xi)) \times \int_0^\theta cos^2\,(\delta_n \eta) d\eta \\ = e^{2\xi} P \int_0^\theta cos\,(\delta_n \eta) d\eta \end{aligned} \tag{38}$$

In general, two non-zero functions $f_i(x)$, $f_j(x)$ are perpendicular when the following relation exists in the $a \le x \le b$ interval:

$$\int_a^b f_i(x).f_j(x) = \begin{cases} 0 & i \ne j \\ c > 0 & i = j \end{cases} \tag{39}$$

Obviously, under the condition, the integral relation becomes:

$$\int_a^b f_i(x).f_i(x)dx = \int_a^b (f_i\,(x))^2 dx > 0 \tag{40}$$

Table 1. values of δ_n for various of ζ and Kn

Kn	**($r_1^*\to 0$)**	**$r_1^*\neq 0$(r_1^*=10μm)**
0.001	-2.997071247	-2.99532911
0.005	-2.985413476	-2.986791194
0.01	-2.970969768	-2.983945293
0.05	-2.970484694	-2.973869919
0.1	-2.970306174	-2.970042528

To solve the integral in Eq.(38), it has to be proven that $\int_0^\theta \cos(\delta_n\eta).\cos(\delta_m\eta)d\eta$ is perpendicular. If $\delta_n = \delta_m$,

$$\int_0^\theta \cos(\delta_n\eta).\cos(\delta_m\eta)d\eta=\int_0^\theta \cos^2(\delta_n\eta)d\eta=$$

$$\int_0^\theta \frac{1+\cos(2\delta_n\eta)}{2}d\eta=\frac{1}{2}(\underbrace{\theta}_{+}+\underbrace{\frac{1}{\underbrace{2\delta_n}_{-}}\underbrace{\sin(2\overbrace{\delta_n}^{-}\overbrace{\theta}^{+})}_{-}}_{+})\succ 0$$

By integrating Eq.(38):

$$X''_n(\xi)-\delta_n{}^2X_n(\xi)=\frac{2sin(\delta_n\theta)}{(\delta_n\theta+sin(\delta_n\theta)cos(\delta_n.\theta))}e^{2\xi}P \qquad (41)$$

Solving Second-order nonhomogeneous differential equation Eq.(41) becomes:

$$X_n(\xi)=c_{n1}e^{(\delta_n\xi)}+c_{n2}e^{(-\delta_n\xi)}-I_1\,e^{2\xi}P \qquad (42)$$

where

$$I_1=\frac{2sin(\delta_n\theta)}{(\delta_n^2-4)(\delta_n\theta+sin(\delta_n\theta)cos(\delta_n.\theta))} \qquad (43)$$

Applying the boundary condition Eqs. (26) and (27):

$$c_{n1}=I_1I_2P \qquad (44)$$

$$c_{n2}=I_1I_3P \qquad (45)$$

Coefficients of $I_2$and I_3 are:

$$I_2=\frac{r_2(\frac{1}{r_1})^{\delta_n}(2\beta Kn+r_2)(1-\frac{\delta_n\beta Kn}{r_1})}{(\frac{r_2}{r_1})^{\delta_n}(1+\frac{\delta_n\beta Kn}{r_2})(1-\frac{\delta_n\beta Kn}{r_1})} \dots\frac{-r_1(\frac{1}{r_2})^{\delta_n}(2\beta Kn+r_1)(1-\frac{\delta_n\beta Kn}{r_2})}{-(\frac{r_1}{r_2})^{\delta_n}(1+\frac{\delta_n\beta Kn}{r_1})(1-\frac{\delta_n\beta Kn}{r_2})} \qquad (46)$$

$$I_3=\frac{r_1r_2{}^{\delta_n}(2\beta Kn+r_1)\left(1+\frac{\delta_n\beta Kn}{r_2}\right)}{(\frac{r_2}{r_1})^{\delta_n}(1+\frac{\delta_n\beta Kn}{r_2})(1-\frac{\delta_n\beta Kn}{r_1})} \dots\frac{-r_2r_1{}^{\delta_n}(2\beta Kn+r_2)\left(1+\frac{\delta_n\beta Kn}{r_1}\right)}{-(\frac{r_1}{r_2})^{\delta_n}(1+\frac{\delta_n\beta Kn}{r_1})(1-\frac{\delta_n\beta Kn}{r_2})} \qquad (47)$$

Substituting Eq.(42) in Eq.(36), velocity equation is obtained:

$$\frac{u(\xi,\eta)}{P}=\sum_{n=1}^{\infty}I_1(I_2e^{(\delta_n\xi)}+I_3e^{(-\delta_n\xi)}-e^{(2\xi)})cos(\delta_n\eta) \qquad (48)$$

The mean velocity is defined in the following expression:

$$u_m=\frac{1}{A_{\xi\eta}}\int udA_{\xi\eta}=\frac{\int_0^\theta\int_{lnr_1}^{lnr_2}ue^{2\xi}d\xi d\eta}{\int_0^\theta\int_{lnr_1}^{lnr_2}e^{2\xi}d\xi d\eta} \qquad (49)$$

Substituting velocity equation in Eq.(49) and integration across the section of the microchannel mean velocity expression leads to:

$$u_m=\sum_{n=1}^{\infty}\frac{2I_1P}{\delta_n\theta}sin(\delta_n\theta)(\frac{I_2}{(\delta_n+2)}(r_2{}^{\delta_n}-r_1{}^{\delta_n})+\frac{I_3}{(-\delta_n+2)}((\frac{1}{r_2})^{\delta_n}-(\frac{1}{r_1})^{\delta_n})-\frac{1}{4}(r_2{}^2+r_1{}^2)) \qquad (50)$$

3. Slip-Flow Models

Poiseuille number is described as the dimensionless mean wall shear stress and depends on hydraulic diameter[12, 13].

$$Po_{L_c}=\frac{(\frac{-A}{perimeter}\frac{dp}{dz})L_c}{\mu u_m}=\frac{fRe_{L_c}}{2} \qquad (51)$$

If Hydraulic diameters are defined:

$$L_c=D_h=\frac{4A}{perimeter} \qquad (52)$$

where A and Perimeter:

$$A=\frac{\theta^*(r_2^{*2}-r_1^{*1})}{2} \qquad (53)$$

$$perimeter=r_2^*(\theta^*+2)+r_1^*(\theta^*-2) \qquad (54)$$

Substituting Eq.(52) and mean velocity Eq.(50) in Eq.(51), the following relationship is obtained:

$$Po=\frac{2\theta(r_2^2-r_1^2)/(r_2(\theta+2)}{\sum_{n=1}^{\infty}\frac{2I_1}{\delta_n\theta}\sin(\delta_n\theta)(\frac{I_2}{(\delta_n+2)}(r_2{}^{\delta_n}-r_1{}^{\delta_n})}\dots\frac{+r_1(\theta-2))^2}{+\frac{I_3}{(-\delta_n+2)}((\frac{1}{r_2})^{\delta_n}-(\frac{1}{r_1})^{\delta_n})-\frac{1}{4}(r_2{}^2+r_1{}^2))} \qquad (55)$$

Duan and Muzychka[12, 13], Duan and Yovanovich[17], Das and Tahmouresi[21] have indicated that the square root of flow area($\sqrt{A}$) is also more appropriate for non-dimensionalizing gaseous slip flows and non-Newtonian flows, respectively. then:

If Hydraulic diameters are defined:

$$L_c = D_h = \sqrt{A} \quad (56)$$

$$Po = \frac{\sqrt{\theta(r_2^2 - r_1^2)}}{\sum_{n=1}^{\infty}\frac{2I_1}{\delta_n\theta}\sin(\delta_n\theta)(\frac{I_2}{(\delta_n+2)}(r_2{}^{\delta_n} - r_1{}^{\delta_n})} \cdots \frac{/\sqrt{2}\left(r_2(\theta+2)+r_1(\theta-2)\right)}{+\frac{I_3}{(-\delta_n+2)}((\frac{1}{r_2})^{\delta_n} - (\frac{1}{r_1})^{\delta_n}) - \frac{1}{4}(r_2{}^2 + r_1{}^2))} \quad (57)$$

To validate the analytical solution, Poiseuille number in Eq.(57) is solved under the conditions:ideal gas (b = 0), $r_1 \to 0$ and $\theta=2\pi$ (Circular microchannel). Eq.(57) (present model) has been validated with analytical solution ideal gaseous slip flow in circular microchannel: Po, Kandikar[34] and Po, Duan[13]. Table 2 compares values of Po between the present study (Eq.(57)) with those of Kandlikar[34] and Duan[13]. The results show that the error percentage is less than 3%. There is a good agreement between the results of the present study(Eq.(57)) and those of Kandikar [34] and Duan [13].

4. Density equation

Van der Waals Equation is one of the important state equations for non-ideal gas(Eq.(58)):

$$p = \rho RT(1 + B\rho + C\rho^2 + D\rho^3) \quad (58)$$

In Eq.(58), coefficients of B, C and D are:

$$B = \left(b - \frac{a}{RT}\right) \quad (59)$$

$$C = b^2 \quad (60)$$

$$D = b^3 \quad (61)$$

$$a = \frac{27}{64}\frac{R^2 T_C{}^2}{P_C} \quad (62)$$

$$b = \frac{RT_C}{8\,P_C} \quad (63)$$

In Eqs.(62) and (63), R, T_C, $P_C$are defined as the specific gas constant, critical temperature, and critical pressure, respectively. The general form of the mass flow rate equation is as follows:

$$u_m = \frac{\dot{m}}{\rho A} \quad (64)$$

Derivation of the sides of equation (58) to z:

$$\frac{dp}{dz} = RT(1 + 2B\rho + 3C\rho^2 + 4D\rho^3)\frac{d\rho}{dz} \quad (65)$$

Substituting Eq (65) in to Eq.(50), mean velocity equation is:

$$u_m = \sum_{n=1}^{\infty}\frac{2I_1}{\delta_n\theta}\sin(\delta_n\theta)(\frac{I_2}{(\delta_n+2)}\left(r_2{}^{\delta_n} - r_1{}^{\delta_n}\right) + \frac{I_3}{(-\delta_n+2)}((\frac{1}{r_2})^{\delta_n} - (\frac{1}{r_1})^{\delta_n}) - \frac{1}{4}(r_2{}^2 + r_1{}^2)) \times \frac{RTA}{\mu}(1 + 2B\rho + 3C\rho^2 + 4D\rho^3)\frac{d\rho}{dz} \quad (66)$$

Replacing Eq.(66) in Eq.(64) and integral in terms z:

$$u_m = \sum_{n=1}^{\infty}\frac{2I_1}{\delta_n\theta}sin(\delta_n\theta)(\frac{I_2}{(\delta_n+2)}(r_2{}^{\delta_n} - r_1{}^{\delta_n}) + \frac{I_3}{(-\delta_n+2)}((\frac{1}{r_2})^{\delta_n} - (\frac{1}{r_1})^{\delta_n}) - \frac{1}{4}(r_2{}^2 + r_1{}^2)) \times \int_{\rho_i}^{\rho}\frac{RTA^2}{\mu}(\rho + 2B\rho^2 + 3C\rho^3 + 4D\rho^4)d\rho = \int_0^L \dot{m}dz \quad (67)$$

Integrating Eq.(67), the following relationship is obtained:

$$\alpha_5\prod^5 + \alpha_4\prod^4 + \alpha_3\prod^3 + \alpha_2\prod^2 = 1/\alpha_1 + \alpha/\alpha_1 \quad (68)$$

Where

$$\alpha_1 = \frac{RT\theta(r_2^{*2} - r_1^{*2})^2}{2\mu\dot{m}L}[\sum_{n=1}^{\infty}\frac{I_1}{\delta_n}sin(\delta_n\theta)(\frac{I_2}{(\delta_n+2)}(r_2{}^{\delta_n} - r_1{}^{\delta_n}) + \frac{I_3}{(-\delta_n+2)}((\frac{1}{r_2})^{\delta_n} - (\frac{1}{r_1})^{\delta_n}) - \frac{1}{4}(r_2{}^2 + r_1{}^2))] \quad (69)$$

$$\prod = \rho/\rho_i \quad (70)$$

$$\alpha_2 = \frac{1}{2}\rho_i^2 \quad (71)$$

$$\alpha_3 = \frac{2}{3}B\rho_i^3 \quad (72)$$

$$\alpha_4 = \frac{3}{4}C\rho_i^4 \quad (73)$$

$$\alpha_5 = \frac{4}{5}D\rho_i^5 \quad (74)$$

$$\alpha/\alpha_1 = \alpha_2 + \alpha_3 + \alpha_4 + \alpha_5 \quad (75)$$

5. Results and Discussion

The assumptions of the flow geometry and the physical properties of carbon dioxide gas are R=188.92(J/Kg. K), μ=1.74×10-7(N.s/m2), ρi=1.517(Kg/m3), =0.002139(m3/Kg), T=350 K, ṁ=5×10-10 (Kg/s), σ=1. Tables 3 and 4 show the values in terms of the microchannel length in different Knudsen numbers (Kn=10-3, Kn=5×10-3, Kn=10-2, Kn=5×10-2, and Kn=10-1) for r1*→0 and r1*≠0 (r1*=10μm), respectively. Dimensions of micro-channel geometry include θ=π/6, r2*=15μm, r1*→0 and r1*≠0 (r1*=10μm), respectively. According to the tables 3 and 4 with the increase in the length of the microchannel at various Knudsen numbers and as well as the increase of Knudsen number in a specified length, the values of the ratio of density to inlet density decrease and increase, respectively. A comparison between the ratio of density to inlet density for r1*→0 and r1*≠0 shows that the values in condition of r1*≠0 (r1*=10μm) are more than r1*→0 for all various length and Knudsen numbers. In other words, the rarefication process of the gas flow in r1*→0 condition is faster than r1*≠0 (r1*=10μm).

According to the results, the rarefication process is a function of the Knudsen number and the cross-section geometry. That way, in a specific length, the rarefication process decreases with increasing Knudsen number and narrowing cross-section geometry (r1*≠0). In gas sensors, the use of circular sector microchannel (r1*≠0) is appropriate because the rarefication process occurs later. In sensors where the rate of rarefication process is important, the use of circular sector microchannel (r1*=0) is appropriate.

Tables 5 and 6 represent the Π values in terms of the microchannel length for various angles in Kn=0.05, $r_1^*\rightarrow 0$ and $r_1^*\neq 0$, respectively. The results show that with the increase of the length of the microchannel at various angles, the values of the ratio of density to inlet density decline. In specified length, the reduction of angles leads to decrease values of Π when $r_1^*\rightarrow 0$ and decreases and then increases when $r_1^*\neq 0$. According to results, in specified length and Knudsen number, when angles decrease, the rate of rarefication process is a function of the cross-section geometry and changing the small radius of the circular sector (r_1^*). In gas sensor, the use of the circular sector microchannel with θ=π/6 and $r_1^*\neq 0$ is appropriate because the rarefication process occurs later.

Table 7 indicates comparison ∏ values between the ideal and non-ideal gaseous slip flow in L=5μm. According to results, for an ideal gas, ∏ values of circular sector microchannel in the condition of $r_1^*\neq 0$ (r_1^*=10μm) is more than $r_1^*\rightarrow 0$. Also, ∏ values of an ideal gas are more than non-ideal gas in different Knudsen numbers. Therefore, the rarefication process of the non-ideal gas is faster than the ideal gas.Then, in gas sensor, it is appropriate to use gases that are closer to behavior of non-ideal gas.

Figs. 2 and 3 show the fully developed velocity profiles in different Knudsen numbers when θ=π/6, $r_1^*\rightarrow 0$ and $r_1^*\neq 0$ (r_1^*=10μm), respectively. According to Figs. 2 and 3 with the increase of the Knudsen number, velocity values increase.In the specified Knudsen number,velocity values increase firstly and then decrease.Also,with increasing Knudsen number,slippage velocity values are more than others. This indicates that an increase of Knudsen number results in the increase of the pressure drop caused by the slip, so that the fluid flow in these microchannels should be within the lower Knudsen number range.

Figs. 4 and 5 show the fully developed velocity profiles in under various angles at Kn=0.05, $r_1^*\rightarrow 0$ and $r_1^*\neq 0$ (r_1^*=10μm), respectively. According to Fig. 4, with the increase of the radius, velocity values increased and then decrease. The maximum velocity is θ=π/9. With decreasing θ, the slippage velocity values increase for $r_1^*\rightarrow 0$. This indicates that the reduction of angle of circular sector micro-channel results in an increase of the micro-channel pressure drop. It is approprate to choose the circular sector microchannel with the maximum angle. In Fig. 5, velocity values have a state of fluctuation when radius increases.

Conclusion

In this paper, the momentum equation is solved for the circular sector microchannel under the fully developed non-ideal gaseous slip flow using the conformal mapping and integral transform technique. It is presented the models for predicting the local and mean velocity, normalized Poiseuille number, and the ratio of density. It was shown that present values of normalized Poiseuille number model are in good agreement for previous results[13, 34] for circular microchannels. Also, the rarefication process is a function of the Knudsen number and the cross-section geometry and is a weak function of the type of gases. Poiseuille number is independent of fluid material properties, velocity, temperature and is a function of the cross-section shape.

Poiseuille number in terms of dimensionless radius for various Knudsen number, $r_1^*\rightarrow 0$, and $r_1^*\neq 0$ (r_1^*=10μm) are shown in Figs. 6 and 7, respectively. Fig. 6 shows that logarithmic function of Poiseuille number decreases with the increase of the radius and also, with the increasing Knudsen number, values of poiseuille decrease. The process of changes is different in Fig. 7. With the increase of the radius Poiseuille numbers increase. According to the fluid flow in the microchannel is assumed laminar, when the friction factor is constant, the using of circular sector microchannel with $r_1^*\neq 0$ (r_1^*=10μm) is appropriate.

Table 2. Comparison of values of $Po_{D_h=\sqrt{A}}$ with those of Kandlikar[34] and Duan[13].

Kn	$Po, D_h=\sqrt{A}$	$Po, Kandlikar[34]$	$Po, Duan[13], r_1=0$	ERROR%
0.001	15.9647412385	15.8730158730	15.87826257	0.57
0.003	15.7392319765	15.625	15.62671297	0.72
0.005	15.5204692019	15.3846153846	15.38562	0.87
0.01	15.0011411590	14.8148148148	14.8152894	1.24
0.03	13.0898901887	12.9032258064	12.90335362	1.42
0.05	11.1613287818	11.4285714285	11.42863455	2.39
0.07	9.95999449826	10.2564102564	10.25644787	2.97
0.1	8.78265117204	8.88888888888	8.888909298	1.2

Table 3. Values of Π in terms of circular sector microchannel length at ($r_1^* \to 0$)

X(mm)	$Kn=10^{-3}$	$Kn=5\times10^{-3}$	$Kn=10^{-2}$	$Kn=5\times10^{-2}$	$Kn=10^{-1}$
0	0.9999984771	0.9999984771	0.9999984771	0.9999984771	0.9999984771
10	0.9731212253	0.9735690615	0.9741081771	0.9777335766	0.9810293946
20	0.9454807317	0.9464023353	0.9475111557	0.9549500393	0.9616864636
30	0.9170079967	0.9184328867	0.9201461441	0.9316098227	0.9419466591
40	0.8876229523	0.8895850205	0.8919424741	0.9076699928	0.9217844897
50	0.8572318039	0.8597703385	0.8628179245	0.8830817956	0.9011716126
100	0.6853629817	0.6916927066	0.6992404091	0.7481228016	0.7900862300

Table 4. Values of Π in terms of circular sector microchannel length at $r_1^*\neq0$(r_1^*=10μm)

X(mm)	$Kn=10^{-3}$	$Kn=5\times10^{-3}$	$Kn=10^{-2}$	$Kn=5\times10^{-2}$	$Kn=10^{-1}$
0	0.9999984771	0.9999984771	0.9999984771	0.9999984771	0.9999984771
10	0.9993270555	0.9993490190	0.9993753977	0.9995502769	0.9997028768
20	0.9986551832	0.9986991392	0.9987519299	0.9991018754	0.9994071891
30	0.9979828584	0.9980488361	0.9981280728	0.9986532731	0.9991114135
40	0.9973100812	0.9973981092	0.9975038259	0.9982044693	0.9988155508
50	0.9966368496	0.9967469583	0.9968791887	0.9977554633	0.9985196005
100	0.9932638527	0.9934848042	0.9937501151	0.9955073994	0.9970385317

Table 5. Values of Π in terms of circular sector microchannel length for various angles at Kn=0.05, $r_1^* \to 0$

X(mm)	θ=π/6	θ=π/7	θ=π/8	θ=π/9
0	0.9999984771	0.9999984771	0.9999984771	0.9999984771
10	0.9777335766	0.9685511429	0.9571799417	0.9433458440
20	0.9549500393	0.9360485842	0.9123553530	0.8830684837
30	0.9316098227	0.9023768090	0.8652130480	0.8183660169
40	0.9076699928	0.8673996925	0.8153511899	0.7480913771
50	0.8830817956	0.8309524481	0.7622363710	0.6704951270
100	0.7481228016	0.6172557240	0.7051340166	0.4789866382

Table 6. Values of Π in terms of circular sector microchannel length for various angles at Kn=0.05, $r_1^*\neq0$ (r_1^*=10μm)

X(mm)	θ=π/6	θ=π/7	θ=π/8	θ=π/9
0	0.9999984771	0.9999984771	0.9999984771	0.9999984771
10	0.9995502769	0.9994715875	0.9994872579	0.9995552796
20	0.9991018754	0.9989444205	0.9989757768	0.9991118852
30	0.9986532731	0.9984169750	0.9984640343	0.9986682945
40	0.9982044693	0.9978892509	0.9979520296	0.9982245068
50	0.9977554633	0.9973612477	0.9974397617	0.9977805219
100	0.9955073994	0.9947170312	0.9948744699	0.9955576282

Table 7. Comparison of ∏ values between ideal and non ideal gaseous flow for first boundary conditions in L=5μm

	Ideal Gas			Non-Ideal Gas		
Microchannel	$Kn=10^{-3}$	$Kn=10^{-2}$	$Kn=10^{-1}$	$Kn=10^{-3}$	$Kn=10^{-2}$	$Kn=10^{-1}$
$r_1^* \to 0$	0.85732662	0.86290902	0.90123742	0.85723180	0.86281792	0.90117161
$r_1^*\neq0$(r_1^*=10μm)	0.99664055	0.99688273	0.99852208	0.99663684	0.99687918	0.99851960

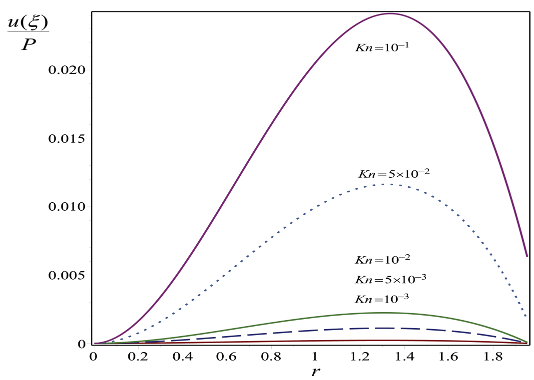

Figure 2. The velocity profile of circular sector microchannel under different Knudsen numbers in θ=π/6 , $r_1^*\to0$

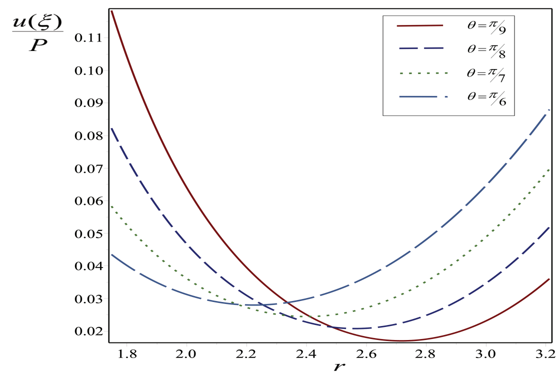

Figure 5. The velocity profile of circular sector microchannel under different angles in Kn=0.05, r1*≠0 (r1*=10μm)

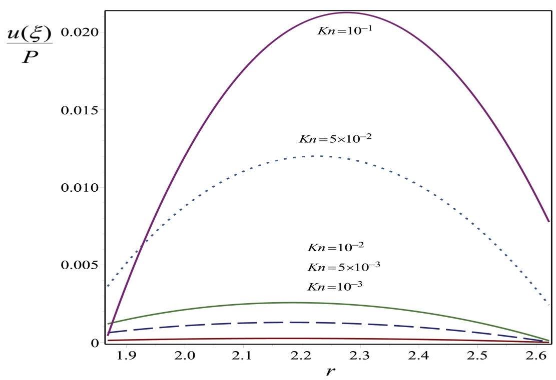

Figure 3. The velocity profile of circular sector microchannel under different Knudsen numbers in θ=π/6, $r_1^*\neq0$ (r_1^*=10μm)

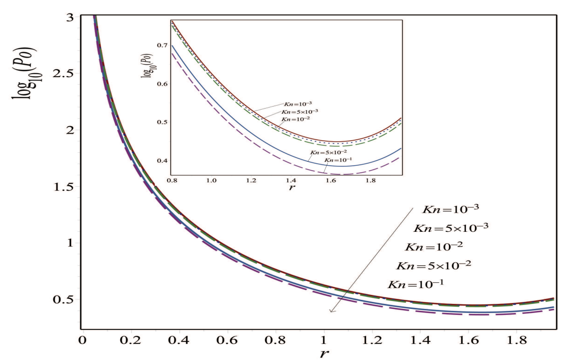

Figure 6. Poiseuille number in terms of dimensionless radius for 10-3 ≤ Kn ≤ 10-1, r1*→0

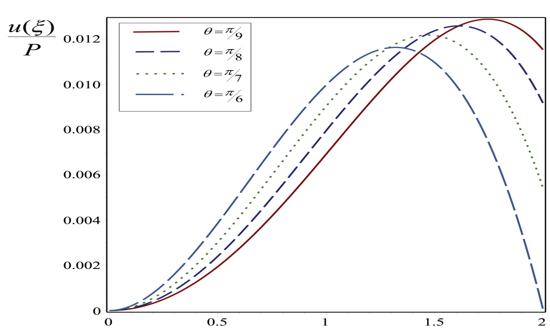

Figure 4. The velocity profile of circular sector microchannel under different angles in Kn=0.05, r1*→0

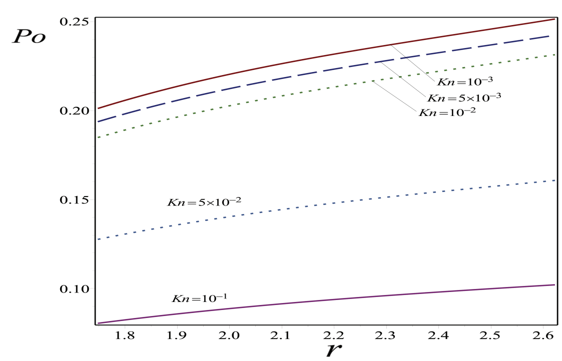

Figure 7. Poiseuille number in terms of dimensionless radius for 10-3 ≤ Kn ≤ 10-1,r1*≠0 (r1*=10μm)

Nomenclature

u	Gaseous velocity component (m/s)
r*, θ*	Polar coordinates (m)
r , θ	Dimenstionless polar coordinates
z	Coordinate in flow direction (m)
x^* , y^*	Cartesian coordinates (m)
x , y	Dimenstionless cartesian coordinates
p	Pressure (N/m^2)
D_h	Hydraulic diameter (m)
r_1	Radius of circular sector microchannel radius (m)
r_2	Radius of circular sector microchannel radius (m)
Kn	Knudsen number (l/D_h)
A_c	Cross – sectional area (m^2)
h	Coefficient
J	Jacobian transform
R	Specific gas constant (J/Kg.K)
T	Temperature (K)
u_m	Mean velocity
$\dot{m}$	Mass flow rate (Kg/s)
Po	Poiseuille number
v_c	Critical Specific Volume

Greek symbols

ρ	Gas density (Kg/m^3)
μ	Dynamic viscosity ($N.s/m^2$)
σ	Tangential momentum accomondation coefficient
λ	Molecular mean free path (m)
ξ, η	Dimenstionless cartesian coordinates
δ	eigenvalue

subscripts

r	r direction
θ	θ direction
z	Z direction
i	inlet

References

[1] ARKILIC, E. B., SCHMIDT, M. & BREUER, K. S. 1997. Gaseous slip ow in long microchannels. *Journal of Microelectromechanical systems.*

[2] EBERT, W. & SPARROW, E. M. 1965. Slip flow in rectangular and annular ducts. *Journal of Basic Engineering,* 87**,** 1018-1024.

[3] ZOHAR, Y., LEE, S. Y. K., LEE, W. Y., JIANG, L. & TONG, P. 2002. Subsonic gas flow in a straight and uniform microchannel. *Journal of fluid mechanics,* 472**,** 125-151.

[4] SHEN, C. 2005. Use of the degenerated Reynolds equation in solving the microchannel flow problem. *Physics of Fluids,* 17**,** 046101.

[5] MORINI, G. L., SPIGA, M. & TARTARINI, P. 2004. The rarefaction effect on the friction factor of gas flow in microchannels. *Superlattices and microstructures,* 35**,** 587-599.

[6] DONGARI, N., AGRAWAL, A. & AGRAWAL, A. 2007. Analytical solution of gaseous slip flow in long microchannels. *International journal of heat and mass transfer,* 50**,** 3411-3421.

[7] AGRAWAL, A. 2012. A comprehensive review on gas flow in microchannels. *International Journal of Micro-Nano Scale Transport*.

[8] DONGARI, N., SHARMA, A. & DURST, F. 2009. Pressure-driven diffusive gas flows in micro-channels: from the Knudsen to the continuum regimes. *Microfluidics and nanofluidics,* 6**,** 679-692.

[9] DONGARI, N., DADZIE, S. K., ZHANG, Y. & REESE, J. M. Isothermal micro-channel gas flow using a hydrodynamic model with dissipative mass flux. AIP Conference Proceedings, 2011. AIP, 718-723.

[10] DONGARI, N., DADZIE, S. K., ZHANG, Y. & REESE, J. M. Isothermal micro-channel gas flow using a hydrodynamic model with dissipative mass flux. AIP Conference Proceedings, 2011. AIP, 718-723.

[11] VIMMR, J., KLÁŠTERKA, H. & HAJŽMAN, M. 2012. Analytical solution of gaseous slip flow between two parallel plates described by the

Oseen equation. *Mathematics and Computers in Simulation,* 82**,** 1832-1840.

[12] DUAN, Z. & MUZYCHKA, Y. 2007a. Slip flow in elliptic microchannels. *International Journal of Thermal Sciences,* 46**,** 1104-1111.

[13] DUAN, Z. & MUZYCHKA, Y. 2007b. Slip flow in non-circular microchannels. *Microfluidics and Nanofluidics,* 3**,** 473-484.

[14] RASHIDI, M., GANJI, D. & SHAHMOHAMADI, H. 2011. Variational iteration method for two-dimensional steady slip flow in micro-channels. *Archive of Applied Mechanics,* 81**,** 1597-1605.

[15] DAS, S. K. & TAHMOURESI, F. 2016. Analytical solution of fully developed gaseous slip flow in elliptic microchannel. *Int. J. Adv. Appl. Math. and Mech. 3i***,** 1-15.

[16] KURKIN, E. I., SAMSONOV, V. N. & SHAKHOV, V. G. 2017. Simulation of Rarefied Gas Flows in Microchannels. *Procedia engineering,* 185**,** 160-167.

[17] DUAN, Z. & YOVANOVICH, M. Models for gaseous slip flow in circular and noncircular microchannels. ASME 2010 8th International Conference on Nanochannels.

[18] IHLE, T. & KROLL, D. 2000. Thermal lattice-Boltzmann method for non-ideal gases with potential energy. *Computer physics communications,* 129**,** 1-12.

[19] REDDY, K. V. & REDDY, M. G. 2014. Velocity slip and joule heating effects on MHD peristaltic flow in a porous medium. *Int. J. Adv. Appl. Math. Mech.,* 2**,** 126-138.

[20] HUANG, H. & LU, X.-Y. 2009. Simulation of Gas Flow in Microtubes by Lattice Boltzmann Method. *International Journal of Modern Physics C,* 20**,** 1145-1153.

[21] TAHMOURESI, F. & DAS, S. K. 2014. Analytical modeling of gaseous slip flow in parabolic microchannels. *Journal of Fluids Engineering,* 136**,** 071201.

[22] HUANG, H., LEE, T. & SHU, C. 2007. Lattice Boltzmann method simulation gas slip flow in long microtubes. *International Journal of Numerical Methods for Heat & Fluid Flow,* 17**,** 587-607.

[23] YANG, Z. & GARIMELLA, S. 2009. Rarefied gas flow in microtubes at different inlet-outlet pressure ratios. *Physics of Fluids,* 21**,** 052005.

[24] HONG, C., NAKAMURA, T., ASAKO, Y. & UENO, I. 2016. Semi-local friction factor of turbulent gas flow through rectangular microchannels. *International Journal of Heat and Mass Transfer,* 98**,** 643-649.

[25] LI, H. & HRNJAK, P. 2017. Effect of channel geometry on flow reversal in microchannel evaporators. *International Journal of Heat and Mass Transfer,* 115**,** 1-10.

[26] LI, H. & HRNJAK, P. 2018. Effect of refrigerant thermophysical properties on flow reversal in microchannel evaporators. *International Journal of Heat and Mass Transfer,* 117**,** 1135-1146.

[27] MONSIVAIS, I., LIZARDI, J. & MÉNDEZ, F. 2018. Conjugate thermal creep flow in a thin microchannel. *International Journal of Thermal Sciences,* 124**,** 227-239.

[28] DAS, S., ALI, A. & JANA, R. N. J. 2016. Slip flow of an optically thin radiating non-Gray couple stress fluid past a stretching sheet. *Journal of Heat and Mass Transfer Research,* 3**,** 21-30.

[29] SAROJAMMA, G., SREELAKSHMI, K. & VASUNDHARA, B. 2017. Unsteady boundary layer flow of a Casson fluid past a wedge with wall slip velocity. *Journal of Heat and Mass Transfer Research,* 4**,** 91-102.

[30] RAHMATI, A. & NAJATI, F. 2018. Analytical solution of pressure driven gas flow and heat transfer in micro-Couette using the Burnett equations. *Journal of Heat and Mass Transfer Research,* 5**,** 87-94.

[31] BARRON, R. F., WANG, X., AMEEL, T. A. & WARRINGTON, R. O. 1997. The Graetz problem extended to slip-flow. *International Journal of Heat and Mass Transfer,* 40**,** 1817-1823.

[32] MAXWELL, J. C. 1879. VII. On stresses in rarified gases arising from inequalities of temperature. *Philosophical Transactions of the royal society of London,* 170**,** 231-256.

[33] WANG, M. & LI, Z. 2007. An Enskog based Monte Carlo method for high Knudsen number non-ideal gas flows. *Computers & fluids,* 36**,** 1291-1297.

[34] KANDLIKAR, S., GARIMELLA, S., LI, D., COLIN, S. & KING, M. R. 2005. *Heat transfer and fluid flow in minichannels and microchannels*, elsevier.